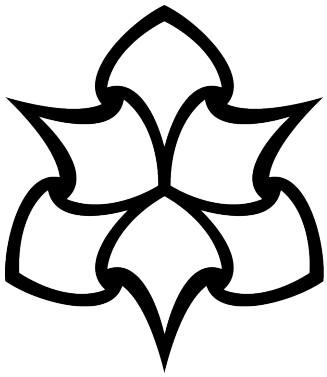

Ultrasound in Med. & Biol., Vol. 00, No. 00, pp. 1–12, 2019

0301-5629/$ - see front matter

https://doi.org/10.1016/j.ultrasmedbio.2019.01.018

● *Original Contribution*

FOREGROUND DETECTION ANALYSIS OF ULTRASOUND IMAGE SEQUENCES IDENTIFIES MARKERS OF MOTOR NEURONE DISEASE ACROSS DIAGNOSTICALLY RELEVANT SKELETAL MUSCLES

KATE BIBBINGS,* PETER J. HARDING,[†,‡] IAN D. LORAM,*
NICHOLAS COMBES,[§] and EMMA F. HODSON-TOLE*

* School of Healthcare Sciences, Manchester Metropolitan University, Manchester, United Kingdom; [†] Crime and Well-Being Big Data Centre, Manchester Metropolitan University, Manchester, United Kingdom; [‡] Elements Technology Platforms Ltd., Cheshire, United Kingdom; and [§] Department of Neurophysiology, Preston Royal Hospital, Lancashire Teaching Hospital Trust, Preston, United Kingdom

(*Received* 27 *September* 2018; *revised* 15 *January* 2019; *in final from* 19 *January* 2019)

Abstract—Diagnosis of motor neurone disease (MND) includes detection of small, involuntary muscle excitations, termed *fasciculations*. There is need to improve diagnosis and monitoring of MND through provision of objective markers of change. Fasciculations are visible in ultrasound image sequences. However, few approaches that objectively measure their occurrence have been proposed; their performance has been evaluated in only a few muscles; and their agreement with the clinical gold standard for fasciculation detection, intramuscular electromyography, has not been tested. We present a new application of adaptive foreground detection using a Gaussian mixture model (GMM), evaluating its accuracy across five skeletal muscles in healthy and MND-affected participants. The GMM provided good to excellent accuracy with the electromyography ground truth (80.17%–92.01%) and was robust to different ultrasound probe orientations. The GMM provides objective measurement of fasciculations in each of the body segments necessary for MND diagnosis and hence could provide a new, clinically relevant disease marker. (E-mail: e.tole@mmu.ac.uk) © **2019 The Author(s). Published by Elsevier Inc. on behalf of World Federation for Ultrasound in Medicine & Biology. This is an open access article under the CC BY-NC-ND license. (http://creativecommons.org/licenses/by-nc-nd/4.0/).**

Key Words: **Amyotrophic lateral sclerosis, Diagnostics, Electromyography, Feature tracking, Gaussian mixture model, Image processing, Myosonography, Neuromuscular, Ultrasonography.**

INTRODUCTION

Motor neurone diseases (MNDs) are characterised by progressive motor neuron degeneration leading to muscle weakness and wasting and reduced mobility, speech, swallowing and respiratory capabilities (Kiernan et al. 2011). These diseases are currently incurable (Baumer et al. 2014; Kiernan et al. 2011). To facilitate trials of new therapeutic interventions there is significant need to identify sensitive markers of neuromuscular degeneration to support early diagnosis and provide sensitive outcome measures of progression (Kiernan et al. 2011). In the wider clinical context, objective markers provide a means of facilitating consistent standards through time and between clinicians, as well as enabling detailed historical records to be established and maintained without additional burden on healthcare staff.

One diagnostic indicator of MND is the occurrence of spontaneous, intermittent, involuntary contractions of muscle fibres, termed *fasciculations*, in multiple muscles across different body regions (de Carvalho et al. 2008). Fasciculation potentials are detected using intramuscular electromyography (EMG) (Mills 2010), which involves insertion of a needle electrode into each muscle to record changes in muscle fibre membrane potential. Although the needles are not dangerous, many patients find them painful and unpleasant; and although the approach is the current clinical gold standard, recent evidence suggests that this method may not be the most sensitive means of detecting fasciculation potentials (Grimm et al. 2015; Misawa et al. 2011).

Address correspondence to: Emma F. Hodson-Tole, Address: School of Healthcare Sciences, Manchester Metropolitan University, John Dalton Building, Oxford Road, Manchester M1 5GD, UK. E-mail: e.tole@mmu.ac.uk

Fasciculations are also visible in ultrasound image sequences as small localised movements (twitches) in the muscle tissue (Walker et al. 1990). It has been reported that ultrasound-based detection of fasciculations has high sensitivity and specificity rates (96% and 84%, respectively) (Arts et al. 2012), and recent work has proposed ultrasound imaging is a valuable additional tool for diagnosis (Grimm et al. 2015; Tsuji et al. 2017). These studies, however, are based on operator identification of the presence or absence of visible twitches in collected image sequences.

Although computational methods of analyzing ultrasound image sequences of skeletal muscles are growing in number (*e.g.,* Darby et al. 2012, 2013; Namburete et al. 2011; Rana and Wakeling 2011; Rana et al. 2009), to our knowledge only one previous report has focused on fasciculation detection (Harding et al. 2016). There, a combination of Lucas−Kanade (LK) feature tracking and mutual information (MI) was used to analyze image sequences. Manual operator identifications of the timing of individual fasciculations was used as ground truth (standard values against which comparisons were made), and the proposed approach had high accuracy (0.83−0.94). However, effective feature tracking requires heterogeneous structure within the image (*i.e.,* clear definition between anatomic features) (Shi and Tomasi 1994). Such structure is only fully evident when the probe is orientated along the long axis of the muscle, so probe orientation could significantly affect algorithm performance. Changes in muscle structure also occur in MND (Maurits et al. 2003) and may have caused the lower agreement found between healthy (0.88−0.94) and MND-affected (0.83−0.84) muscles (Harding et al. 2016). Other physiologic movements (*e.g.,* blood vessel pulsation) can also be detected and not disregarded, because the MI metric peaks during any coherent movement (Harding et al. 2012). This may prove more problematic for muscles in the thoracic/trunk region where additional movements, such as those caused by breathing, may be evident in image sequences and in which the feature tracking/MI approach is currently untested.

We therefore propose an alternative means of detecting fasciculations in ultrasound images; foreground detection using a Gaussian mixture model (GMM). To our knowledge, this algorithm has not previously been applied to medical image sequences, having mainly been used to detect anomalous motion in surveillance images. GMM has been reported to be adaptive and robust to noise (Kaewtrakulpong and Bowden 2001), making it a good candidate for distinguishing between fasciculations and stationary muscle tissue across different muscles, as well as other phenomena such as blood vessel pulsation, breathing patterns and probe motion.

The objectives of this study were therefore (i) to evaluate the accuracy of GMM and the previously reported feature tracking/MI technique to a previously unused, but clinically relevant, ground truth taken from intramuscular EMG signals; and (ii) to determine how GMM-based fasciculation detection performs in comparison to the previously reported feature tracking/MI technique across a range of skeletal muscles commonly assessed for MND diagnosis.

METHODS

Participants

Twenty patients who had previously been diagnosed with probable or definite amyotrophic lateral sclerosis (ALS, the most common form of MND) (Table 1) were recruited through Royal Preston Hospital. Twenty participants self-declared free from any neurologic disorders (54 ± 20 y, 168.8 ± 11.4 cm, 79.0 ± 18.1 kg) were also recruited for comparison. The study was approved by both the local ethics committee in the Faculty of Science and Engineering at Manchester Metropolitan University and the National Research Ethics Service Committee; written consent was obtained from all participants before their inclusion in the study in accordance with the World Medical Association Declaration of Helsinki (2008).

Data acquisition

Ultrasound and EMG data were collected from five muscles: *Gastrocnemius medialis*, *Biceps brachii*, cervical portion of *Trapezius*, *Rectus abdominis* and thoracic paraspinals at the level of T5. These muscles represent each of the body regions that must be assessed to make a confident diagnosis of MND (de Carvalho et al. 2008): (i) upper limb/cervical (*Biceps brachii*); (ii) lower limb/lumbosacral (*Gastrocnemius medialis*); (iii) cranial (*Trapezius*); and (iv) thoracoabdominal (*Rectus abdominis* and thoracic paraspinals). Ultrasound image sequences (approx. 82 fps) were collected using a linear probe (8-MHz frequency, 59 mm long, LogicScan 128, Telemed Ltd, Vilnius, Vilnius County, Lithuania). The probe was manually held, with light contact on the skin surface, alongside a concentric needle electrode (37 mm long, 0.46 mm in diameter, 0.07-mm^2 recording area, Natus Teca, Middleton, WI, USA) that had been inserted into the muscle.

Four 35-s trials were collected from each muscle, with the ultrasound probe positioned in either longitudinal (two trials) or transverse (two trials) orientations relative to the long axis of the muscle, while participants were asked to remain still and relaxed. Ultrasound and EMG data collection were initialized simultaneously using the rising edge trigger output from the ultrasound

Table 1. Details of participants diagnosed with motor neurone disease

Participant	Age (y)	Height (m)	Weight (kg)	Time since diagnosis (mo)
1	55	1.77	92	37
2	62	1.71	110	27
3	71	1.76	69	31
4	72	1.60	57	5
5	41	1.60	64	8
6	59	1.81	88	15
7	84	1.70	90	63
8	71	1.72	84	41
9	79	1.72	67	6
10	83	1.70	70	13
11	70	1.77	82	4
12	54	1.70	66	143
13	71	1.77	80	12
14	65	1.73	90	18
15	52	1.67	—	4
16	74	1.49	57	28
17	73	1.75	102	72
18	55	1.88	102	25
19	64	1.58	85	13
20	71	1.65	79	3
Mean ± SD	64 ± 11	1.70 ± 0.09	80.75 ± 15.30	28 ± 33

SD = standard deviation.

device. EMG signals were amplified (× 1000, Dantec Keypoint Classic system, Optima Medical, Guildford, Surrey, UK) and recorded at 48 kHz using the MATLAB 2013 data acquisition toolbox (The MathWorks, Natick, MA, USA) and a USB data acquisition device (X Series-USB 6341, National Instruments, Austin, TX, USA).

Data analysis

Identification of fasciculations in EMG signals to provide a ground truth signal. The recorded EMG signals were analysed to provide a ground truth signal against which the ultrasound-identified fasciculation events could be compared. Initially, recorded signals were bandpass filtered (fourth-order Butterworth, 30- to 500-Hz cutoff) to remove non-physiologic noise such as movement artefacts. Visual inspection of signals revealed that in some trials, voluntary activation, defined as repeated, regular firing of motor units, had occurred (Fig. 1b, c). To ensure the EMG signal only contained evidence of fasciculation events (sporadic, irregular motor unit firing), motor unit action potentials associated with voluntary activation were identified and removed from the signals using a template matching approach implemented with a freely available software (EMGlab 1.03) (McGill et al. 1985) (Fig. 1d, e).

Because of the sporadic nature and often-complex shape of fasciculation potentials (Fig. 1f), the template matching approach could not be used to identify their timing. We therefore applied thresholding to identify the timing of fasciculation potentials in recorded EMGs. As all trials used to determine an appropriate threshold were removed from further analysis, we attempted to maximise the data taken forward from patient populations (Harding et al. 2016). Therefore, for *Gastrocnemius medialis* and *Biceps brachii*, seven randomly selected trials from the healthy participant data set were used to define the threshold. For the other muscles, however, trials from a third of MND-affected participants were used as very few fasciculations were detected in the healthy data set. Multiples of the absolute mean of the signal providing the best accuracy between thresholded and original EMG signals were identified, with accuracy defined as the area under the receiver operating characteristic (ROC) curve constructed from the two signals. A threshold of 12 was used for all muscles except thoracic paraspinals, for which a value of 10 was optimum.

Identification of fasciculations in ultrasound image sequences. Before analysis, ultrasound images were manually cropped to the lower aponeuroses of the superficial muscle to remove any muscles deep to those containing the EMG needle. This was done to limit the false-positive rate that could have occurred because of the ultrasound potentially detecting fasciculations across multiple muscle layers, while the EMG needle detected potentials over a more restricted muscle volume. Two separate algorithms were then applied to all image data: the previously described feature tracking/MI approach (Harding et al. 2016) and the newly proposed GMM approach, both implemented in MATLAB 2013 using the Image Processing toolbox.

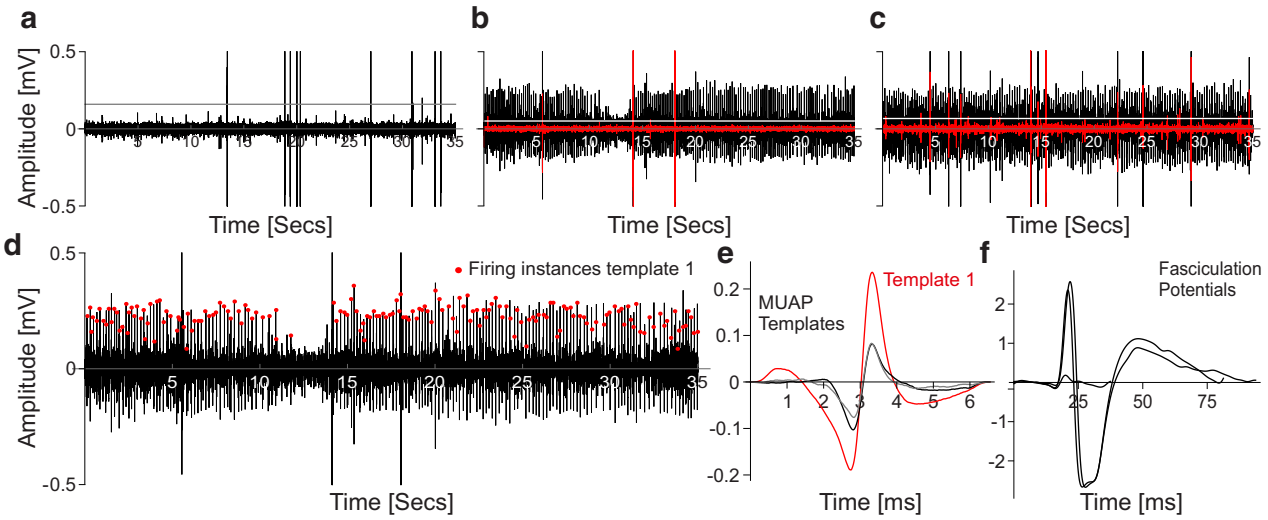

Fig. 1. Examples of collected EMG signals without (a) and with (b and c) background voluntary activity. In (b) and (c), voluntary activity was removed using template matching, and the residual signal is shown in *red*. The *solid horizontal line* in (a)−(c) represents the threshold value used to identify fasciculation potentials. (d) Larger representation of the EMG signal in (b), with the firing instances of one unit denoted (*red dots*). Three representative examples of MUAP templates identified in the signal are provided (e), with template 1 (*red*) related to the firing instances in (d). The fasciculation potentials (f) exhibit more varied shapes than the MUAPs that, along with their sporadic occurrence, meant they were not identifiable using template matching approaches. EMG = electromyography; MUAP = motor unit action potential.

Application of feature tracking and mutual information (LK/MI) approach. According to the methods of Harding et al. (2016), Lucas−Kanade feature tracking (Lucas and Kanade 1981) was applied to provide vectors describing the magnitude and direction of displacement of each image feature between two consecutive images. An 80 × 100-feature grid (with 25 × 25-feature window) was defined in each image *N,* and a Newton−Raphson iterative search for the position of each feature in image $N+1$ was completed. Iterations continued until the feature movement fell below the minimum movement threshold (0.1 pixel) or the change in feature template intensity indicated the new region could not be considered the original feature.

Feature tracking provided a 2-D vector grid quantifying magnitude and displacement of each feature between images. We then used MI to determine the likelihood that the feature displacement between images resulted from a muscle twitch. The approach assumes that the magnitude and direction of any feature movement will be greater, more uniform and coherent (*i.e.,* structured and predictable) around a twitch event than when the muscle is "quiet," when displacements are expected to be more random and mostly influenced by the speckle noise in the images (Harding et al. 2016). The MI of the magnitude and the direction of feature displacement, calculated from their joint and individual probability distributions, provides a measure of the amount of information gained about one signal (*e.g.,* displacement magnitude) when the other (*e.g.,* displacement direction) is known, and *vice versa*. MI was therefore calculated from the feature tracking results of each of the recorded ultrasound image sequences. As in the original work (Harding et al. 2016), a windowing factor of 5 was applied to resulting MI signals to improve the signal-to-noise ratio, providing a 1-D signal in which peaks were considered to represent muscle twitches resulting from fasciculation.

Application of GMM foreground detection approach. Foreground detection using GMM works on the assumption that the background portion of an image sequence will be more frequently visible than any foreground objects and that its pixels will have low variance (Kaewtrakulpong and Bowden 2001). In applying this approach to ultrasound images, we assume that the intensity values of each pixel will vary little when the muscle is quiet. A muscle twitch results in localized disturbance of muscle tissue (Pillen et al. 2008; Walker et al. 1990). Therefore, it is predicted that during a twitch event, transient variations in intensity values will occur in pixels located in the image region in which the twitch occurred and that these will return to baseline values, consistent with the remainder (or background) of the image after the twitch.

Gaussian mixture model foreground detection was applied using the approach of Kaewtrakulpong and Bowden (2001) (see the Appendix). The first step was to use a series of training images (first 300−500 images of the trial,

Table 2. Parameters used for Gaussian mixture model analysis for each muscle and probe orientation

Muscle	Probe orientation	No. of Gaussians	Background ratio*	Learning rate	No. of training frames	Minimum object area*
Biceps brachii	L	5	85	0.5	500	20
	T	3	80	0.5	500	15
Gastrocnemius medialis	L	5	90	0.05	500	15
	T	3	85	0.05	500	20
Trapezius	L	3	90	0.5	500	10
	T	4	90	0.05	500	10
Rectus abdominis	L	5	90	0.05	500	10
	T	5	90	0.05	500	10
Thoracic paraspinal	L	3	90	0.005	300	10
	T	3	90	0.005	100	8

L = longitudinal; T = transverse.
*Background ratios and minimum object areas are reported as percentages of the image area.

Table 2) to establish a mixture of K Gaussians that model every pixel's intensity values across the selected images (Fig. 2). Each K distribution is weighted based on the proportion of the image sequence its intensities occur in the image. The K distributions are ordered (greatest to least weighting). The first distributions determine which pixel intensity values should be considered background, based on a threshold value that sets the minimum amount of the image that should be identified as background (Table 2).

Next the pixel values in the remaining images in the sequence are evaluated in a process that uses the established mixture of K Gaussians, but also updates the model using a pre-defined learning rate (Table 2), so that the model adapts to the occurrence of any repeating changes in intensity values (*e.g.,* related to blood vessel pulsation, probe movement). At the end of this process, it is possible to identify, for each pixel, the frames in which the intensity values lie within the first distributions and can be considered to represent the background and frames in which values lie within the lower-order distributions, considered to represent foreground.

As fasciculations are typically spatially localized within the muscle, we expect that frames in which a twitch event occurs will contain a number of foreground pixels, spatially localized within the image rather than sparsely distributed across the image. To identify clusters of foreground pixels, termed *foreground objects*, the density distribution of the foreground pixels was analysed using

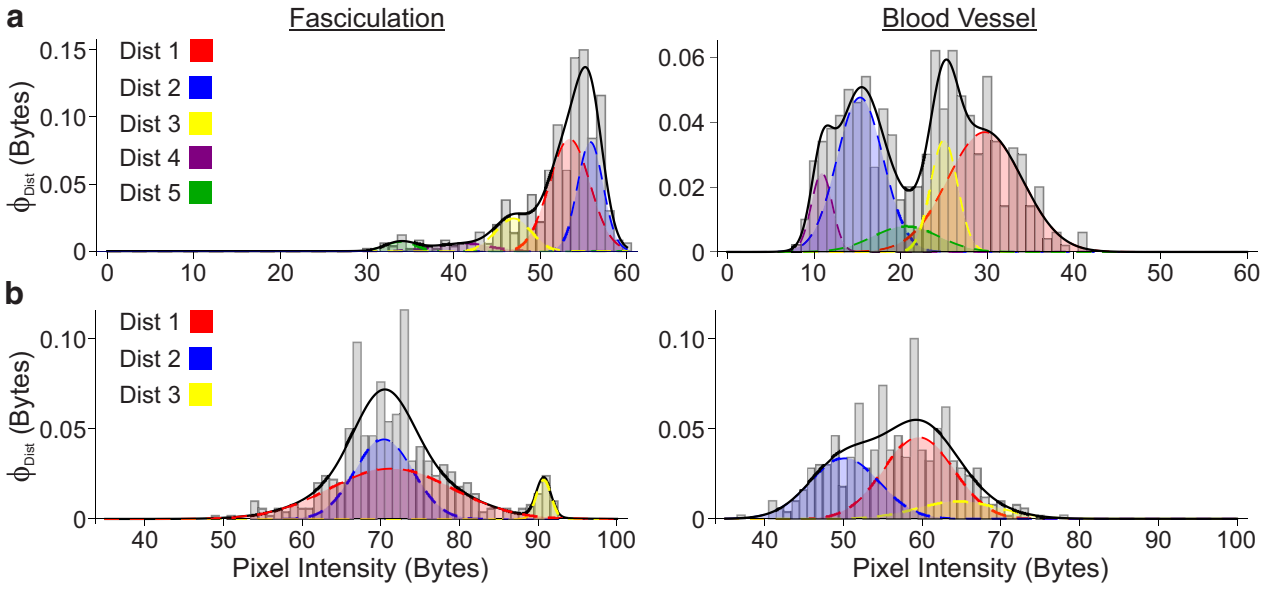

Fig. 2. Example Gaussian mixture models taken from intensity values of pixels in image sequences collected from *Gastrocnemius medialis* with the probe in longitudinal (a) and transverse (b) orientation. Each panel on the left contains data from a pixel located in a region influenced by a fasciculation event (operator confirmed). Panels on the right are from a pixel located in a region where a blood vessel was evident. Note how the mixture of Gaussians enables the different pixel intensity distributions to be described and how the lowest-weighted distributions occupy a different space compared with the higher-weighted ones for pixels in the region of a fasciculation.

Table 3. Parameters used for Lucas–Kanade/mutual information analysis of the limb muscles

Probe orientation	*Biceps brachii*		*Gastrocnemius medialis*	
	Longitudinal	Transverse	Longitudinal	Transverse
Motion direction	$\pi/2$	$\pi/2$	$\pi/8$	$\pi/4$
Displacement	3	3	8	4

connective components. Areas of foreground pixels greater than a minimum value (Table 2) are classed as foreground objects, with all other, more sparsely distributed, foreground pixels disregarded (Stauffer and Grimson 1999). The final result was therefore a 1-D signal of the number of foreground objects at each time point (image frame).

Although it may not hold that individual pixel intensity values in an image sequence will follow a Gaussian distribution (Wagner et al. 1983), using a mixture of Gaussian distributions should enable approximation of the statistical distributions of the pixel intensity values across the image sequence (Fig. 2). Given the transient nature of pixel intensity changes during a twitch event, we therefore hypothesized that the GMM is applicable for detection of fasciculations, with twitch events expected to result in detection of foreground objects and no twitch events detected when the muscle was quiet.

Algorithm parameterisation. Both of the image analysis approaches contain parameters that require optimisation before application. For the limb muscles, *Biceps brachii* and *Gastrocnemius medialis,* approximately one-third of the unaffected participant group were randomly selected for parameterisation, with their data removed from the final analysis, so that algorithm evaluation was performed on previously unseen data. Only unaffected participants were used for this process, to maximise data retained from the patient group. For the three trunk muscles, too few fasciculations were identified in healthy participants to provide data for parameterisation. Therefore, one-third of MND-affected data were used for parameterisation and again removed from final analysis. Separate optimisation was completed for each muscle and probe orientation. The parameter values used in each approach are listed in Tables 2 and 3.

Comparison of image-based detection of fasciculations with ground truth (EMG) signal. EMG-detected fasciculation potentials and the resulting tissue displacement presented in the ultrasound data occur over different timescales (*e.g.,* approx 10 ms [Mills 2010] for fasciculation potentials and 500 ms [Walker et al. 1990] for twitch contraction). Therefore, to ensure a fair comparison, the start and end of each twitch in ultrasound-derived signals were determined by locating the points at which the peaks fell below the noise level. If a fasciculation potential occurred within the period of a twitch, the logical EMG signal was adjusted so the whole twitch epoch was classified as a single, positive event.

The ultrasound device used does not operate with a constant interframe interval, but does provide exact timings of each individual frame collected (Miguez et al. 2017). The GMM and LK/MI signals were therefore interpolated based on the exact frame times so that a direct comparison with the myoelectric time series could be completed. There was also a 30-ms delay between the initiation of the trial and the collection of the first ultrasound image, so data from the first 37.5 ms (equivalent to 3 ultrasound frames) of EMG data were discarded to ensure appropriate alignment between the two signals.

Once both the ultrasound-derived and the EMG-derived fasciculation signals had been obtained, statistical analyses in the form of ROCs were performed (Hanley and McNeil 1982). The area under the curve was used as the measure of accuracy to determine performance of each image analysis technique across muscle and probe orientations in unaffected and MND-affected groups.

RESULTS

Evaluation of limb muscles: Biceps brachii *and* Gastrocnemius medialis

Details of the numbers of fasciculation potentials identified in recorded EMG signals are provided in Table 4. With respect to the performance of the ultrasound-derived fasciculation metrics in unaffected participants, accuracy varied between muscle, probe orientation and the method of image analysis used (Fig. 3). Good accuracy values were found for the GMM approach across all conditions (82.36%–90.31%). The LK/MI had the highest accuracy in the analysis of the *Gastrocnemius medialis* with a transverse probe orientation (78.80 %), with all other values lower (69.62%–78.42 %). The difference in accuracy between probe orientations was between ~0.4 and 7 percentage points in *Gastrocnemius medialis* and *Biceps brachii*, respectively.

Results from MND-affected participants followed a pattern similar to that of the unaffected group (Fig. 3). The GMM gave accuracy values between 84.05% and

Table 4. Numbers of fasciculations detected by EMG ground truth signal in each muscle/participant group*

Muscle	Participant group	Probe orientation	No. detected by EMG
Biceps brachii	Healthy	L	98
	Healthy	T	141
	MND	L	507
	MND	T	242
Gastrocnemius medialis	Healthy	L	172
	Healthy	T	224
	MND	L	437
	MND	T	433
Trapezius	MND	L	466
	MND	T	349
Rectus abdominis	MND	L	42
	MND	T	68
Thoracic paraspinal	MND	L	128
	MND	T	97

EMG = electromyography; L = longitudinal; MND = motor neurone disease; T = transverse.
*In trunk muscles, no EMG fasciculations were recorded in healthy participants, a feature common in recent reports (Tsuji et al. 2017) and current diagnostic criteria.

87.05%. Between *Gastrocnemius medialis* and *Biceps brachii*, differences of up to 3 percentage points occurred. The LK/MI again provided greatest accuracy in *Gastrocnemius medialis* with the probe in transverse orientation (77.72 %); all other results were, however, lower (69.23%−76.21%). Within each muscle, probe orientation affected accuracy with differences of ∼2 percentage points occurring.

Evaluation of trunk muscles: Trapezius, Rectus abdominis *and thoracic paraspinals*

Two problems were encountered when evaluating data collected from the trunk muscles. Firstly, very few fasciculation potentials occurred in the healthy participants in these muscles. This meant a ground truth signal was not available for healthy participants, so only data from MND-affected participants have been evaluated. Secondly, analysis of the LK/MI signal from these muscles revealed that, as predicted, oscillations relating to patients' breathing obscured any peaks resulting from fasciculations (Fig. 4; Supplementary Material, online only). As such, it was not possible to construct meaningful ROCs for the LK/MI data, and only the data from GMM approach are presented (Fig. 5).

Details of the numbers of fasciculation potentials identified in recorded EMG signals are given in Table 4. Evaluation of the GMM again revealed good accuracy (80.17%−92.01%). The lowest accuracy occurred in data from *Trapezius* (Fig. 5), although a high number of fasciculation potentials were detected in this muscle. The greatest accuracy was found in *Rectus abdominis* with the probe in longitudinal orientation (Fig. 5), representing the best accuracy for GMM data across all five muscles studied.

In these trunk muscles probe orientation had a larger effect on accuracy (∼4 percentage points, Fig. 5) than was apparent in the limb muscles (∼1 percentage point, Fig. 3). In *Trapezius* and *Rectus abdominis*, accuracy was better with the probe orientated along the long axis of the muscle (longitudinal); in the paraspinal muscles, better accuracy was found with the probe across the long axis of the muscle (transverse).

DISCUSSION

To our knowledge this is the first report of a computational image analysis approach that can detect

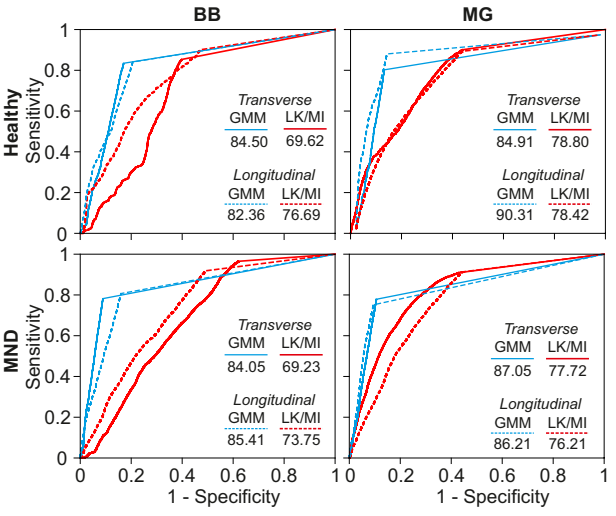

Fig. 3. Receiver operating characteristic curves of Gaussian mixture model (*blue*) and Lucas−Kanade/mutual information (*red*) analysis approaches in *Biceps brachii* (BB, Left) and *Gastrocnemius medialis* (MG, Right) for different probe orientations (transverse: *solid line*, longitudinal: *dashed line*) in healthy (top) and patient (bottom) populations compared with the myoelectric truth signal. GMM = Gaussian mixture model; LK/MI = Lucas−Kanade/mutual information.

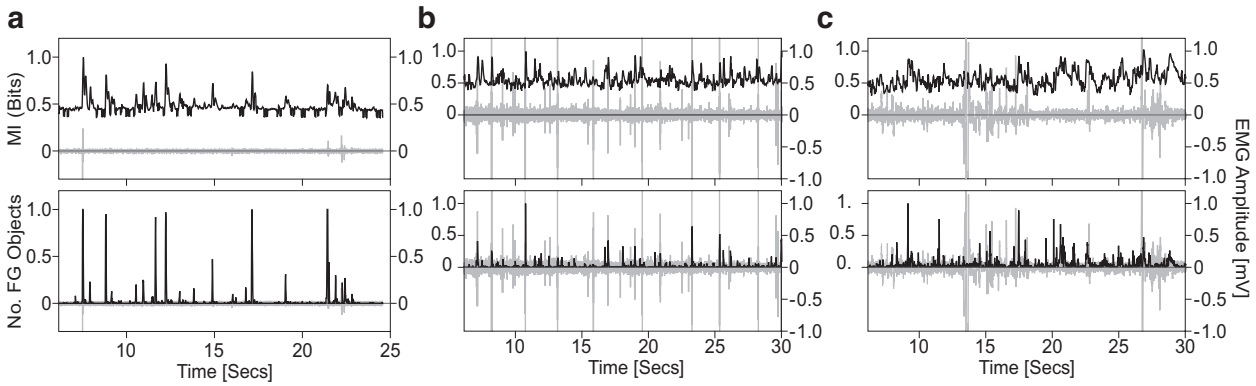

Fig. 4. Example results from LK/MI (top) and GMM (bottom) approaches (black lines) illustrating (a) good agreement between the two signals from *Gastrocnemius medialis* with easily detectable peaks in both signals (also see Supplementary Video S1, online only); (b, c) clear peaks in GMM but noisy and indistinct peaks from LK/MI approach resulting from breathing patterns affecting *Trapezius* (b, also see Supplementary Video S2, online only) and *Rectus abdominis* (c, also see Video 3). Number of foreground objects detected by the GMM has been normalized to one to facilitate display on the same scale as the EMG (grey lines) data, the scale of which is denoted by the axis on the right of each graph. EMG = electromyography; FG = foreground; GMM = Gaussian mixture model; LK/MI = Lucas–Kanade/mutual information.

fasciculations in ultrasound image sequences from muscles in each of the body segments necessary to diagnose MND (de Carvalho et al. 2008). The most important finding was the successful application of the GMM approach to *all* the muscles assessed, with its ability to cope with breathing patterns found in the trunk muscles (Fig. 4; Supplementary Videos S2 and S3, online only). Therefore, our hypothesis that the approach is applicable for fasciculation detection holds true, even when additional physiologic phenomena are present in analysed image sequences.

The high accuracy of the GMM approach (Figs. 3 and 5) is likely due to its adaptive nature and robustness to noise (Kaewtrakulpong and Bowden 2001), which will help it account for factors that could introduce noise into the data, such as operator-induced probe movements. As the number and frequency of fasciculation events can be extracted from the GMM data, there is now the possibility to provide objective measures of fasciculation occurrence in ultrasound image sequences recorded from a range of diagnostically relevant muscles that could be consistently recorded through time and between clinicians and clinics.

How can computational image analysis aid diagnosis and monitoring in MND?

The potential utility of ultrasound for diagnosis of MND is becoming more and more apparent. This is evidenced by the proposal of a "fasciculation ultrasound score" (number of muscles with fasciculations detected) that can sensitively and specifically differentiate ALS and non-ALS patients (Tsuji et al. 2017) and by studies highlighting muscles in which ultrasound is more sensitive for detection of fasciculations than EMG (Grimm et

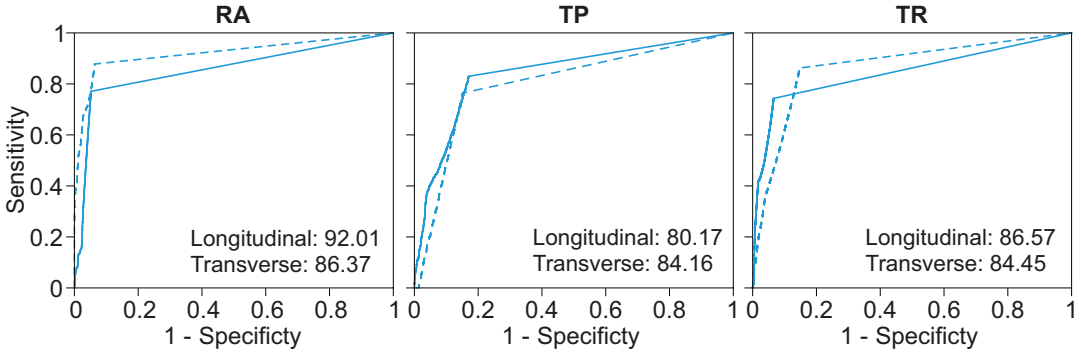

Fig. 5. Receiver operating characteristic curves of Gaussian mixture model analysis approaches in *Rectus abdominis* (RA), thoracic paraspinals (TP) and *Trapezius* (TR) for different probe orientations (transverse: *solid line,* longitudinal: *dashed line*) in the patient population compared with the myoelectric truth signal.

al. 2015; Misawa et al. 2011; Walker et al. 1990). As such, the combination of EMG and ultrasound can, with high sensitively and specificity, be used to evaluate lower motor neuron characteristics, whilst reducing the use of often painful and uncomfortable EMG examinations (Grimm et al. 2015).

There are still, however, challenges in the path of fully exploiting the potential value of muscle ultrasound imaging for clinical applications. These include standardising procedures for collection and analysis of images and levels of inter- and intra-rater agreement. Although the few studies that have assessed inter-rater agreement have found good levels of agreement (Harding et al. 2016; Krämer et al. 2014; Reimers et al. 1996), only small numbers of raters have been used (between 2 and 11). Objective measures of fasciculation occurrence, as provided by the GMM approach, provide the possibility of promoting consistency and standardising ultrasound-based fasciculation detection.

The requirement for evidence of fasciculation potentials within the diagnostic criteria for MND (de Carvalho et al. 2008) highlights its value as a diagnostic marker, although it is also a non-specific finding in many other conditions. Ultrasound imaging has provided evidence that the number of muscles in which fasciculations are found is significantly greater in ALS than in non-ALS patients (Johansson et al. 2017; Tsuji et al. 2017). As these studies have not measured the number or frequency of fasciculations in individual muscles, it is not yet known whether such measures may also be a valuable discriminating feature. However, recent evidence suggests that such measures are important. Specifically, fasciculation number has been positively correlated with rate of disease progression in ALS, while evidence of cortical hyperexcitability together with high fasciculation intensity was a marker of faster disease progression in ALS (Tsugawa et al. 2018). Equally, fasciculation interval has also been suggested as a useful diagnostic measure in ALS (Noto et al. 2017). For these types of measures to be feasibly extracted and robustly evaluated using larger data sets, computational image analysis approaches are required. GMM-based detection of fasciculations is the first such approach now tested for such purposes.

It is suggested that the number of fasciculations declines with disease progression (Takamatsu et al. 2016) and can be transiently affected by additional factors such as strenuous exercise (Fermont et al. 2010). However, there is also evidence that the number of fasciculations is stable over a period of months despite decline in the number of functional motor units (de Carvalho and Swash 2016). Computational analysis of images does not, however, have to be limited to identifying number or frequency of fasciculations. The data available from GMM analysis (*e.g.,* foreground object number and distribution) can also be used to quantify temporal and spatial characteristics of fasciculation events. Such measures could be additionally revealing of changes in dynamic muscle tissue properties associated with motor unit loss, with potential to provide novel markers for patient stratification and monitoring of disease progression.

Limitations and considerations for future work

Both the ultrasound analysis approaches and the detection of fasciculations in the EMG signal required some form of parameterisation. We have tried to maximise the patient-derived data retained for evaluation by parameterising on data from healthy individuals whenever possible. However, the data set is from a relatively small pool of participants. The GMM parameters used may therefore not be generalizable across new data. Future work should thus determine the wider applicability of the parameters used and, if necessary, identify standardised values.

Parameterising on relatively small data sets may also have consequences for the results presented, with the potential that the approaches may be *better* at fasciculation detection than our findings suggest. Specifically, the thresholding values used for the EMG data (Fig. 1) may have allowed some instances of voluntary activation to be wrongly identified as fasciculation events. If EMG spikes related to voluntary activity have been included, this would mean the evaluation has potentially underestimated the performance of the ultrasound metrics. We were unable to identify an alternative method for fasciculation potential detection that could be consistently applied without increasing the potential of operator-based bias (*e.g.,* manually setting individual thresholds per trial). Therefore, although intramuscular EMG is the current clinical standard for fasciculation detection, it is valuable to note that there are challenges associated with using such signals for evaluation of algorithm performance.

A further consideration for the use of intramuscular EMG as a ground truth is the small signal detection volume afforded by the needle electrode. In the presented work, the images were cropped to below the deep aponeurosis of the muscle in which the EMG electrode was placed. This was done to ensure that only tissue displacements in the muscle from which EMG data were recorded were assessed. It is, however, possible that tissue displacements in the very superficial portion of the deeper muscle, potentially interacting with the aponeurosis (see Supplementary Video S1, online only), may have been captured and counted as false-positive events in the ultrasound analysis. This again means the true performance of the image analysis approaches in detecting

fasciculation events has been underestimated in the results presented.

It is important to consider that the occurrence of large numbers of fasciculations within any individual trial may potentially negatively affect the performance of the foreground detection approach. As the algorithm is adaptive, with a parameterised learning rate (Table 2), the occurrence of frequent fasciculations in the same region of the muscle could lead to the associated pixel intensity values being incorporated into the background model and hence no longer being detected. Fasciculation potentials are characterised as being irregular, sporadic motor unit firing (de Carvalho et al. 2008), that are temporally and physically distinct in their electrophysiological characteristics. Although the excitation of motor units leads to distinct signatures in the myoelectric signals, the key question is whether the resulting motor unit activation *also* results in unique signatures in the subsequent tissue displacements that are captured by the ultrasound data. If they do, the adaptive nature of the GMM approach can be viewed as a consistent strength, enabling it to be applied across different muscles and maintaining its robustness in the face of abundant fasciculations. If this is not the case, GMM performance may be reduced by the frequency of fasciculation events.

To fully address the questions noted above requires the relationship between the information content in EMG and ultrasound-based modalities to be more extensively evaluated. Given the small detection volume of concentric needle electrodes, particularly in larger muscles, this will be difficult to do well using recordings similar to those presented here. Such work would, however, benefit from the use of surface electrode arrays, particularly those designed to enable simultaneous recording of EMG and ultrasound from the same portion of muscle (*e.g.,* Botter et al. 2013; Jahanmiri-Nezhad et al. 2014). This could enable factors relating to muscle morphology and source location of fasciculation potentials to be assessed, with such work informing further development of the hybrid diagnostic approaches currently recommend in the literature (Grimm et al. 2015; Misawa et al. 2011).

CONCLUSIONS

The work presented here provides the first evidence that a computational ultrasound image analysis approach, foreground detection using GMMs, can robustly detect fasciculation events in muscles located in each of the body segments required for diagnosis of MND. The selective GMM-based foreground detection analysis should be evaluated over an even wider range of muscles (*e.g.,* including genioglossus) and across a larger patient cohort. Non-invasive objective measures of fasciculation occurrence are now feasible and could facilitate development and maintenance of more detailed patient records and longitudinal studies of changes in fasciculation characteristics to determine potential contributions to monitoring disease progression.

Acknowledgments—This work was supported by funding from the Motor Neurone Disease Association (Grant Ref.: Hodson-Tole/Oct12/866-792). Our thanks also go to the staff and patients at Royal Preston Hospital, Lancashire Teaching Hospitals Trust, for their time.

SUPPLEMENTARY MATERIALS

Supplementary material related to this article can be found online at doi:10.1016/j.ultrasmedbio.2019.01.018.

APPENDIX: DETAILS OF GMM FOREGROUND DETECTION APPROACH

The first 300−500 training images (Table 2) from the start of each image sequence were used as training data to establish a mixture of K Gaussians that model every pixel's intensity value (X) across the image set (Fig. 2). Each tissue surface that comes into the pixel view is therefore represented by a set of states $k \in \{1, 2, \ldots, K\}$. The K Gaussian distributions have parameter sets θ_k, one for each state:

$$\eta(X|\theta_k) = \eta\left(X|\mu_k, \sum_k\right) = \frac{1}{(2\pi)^{1/2}\left|\sum_k\right|^{1/2}} e^{-\frac{1}{2}(X-\mu_k)^T \sum_k^{-1}(X-\mu_k)} \quad \text{(A1)}$$

Here μ_k is the mean and Σ_k is the covariance matrix of the kth distribution. The probability that a pixel has an intensity value of X_t at time t is therefore given by

$$P(X_t) = \sum_{k=1}^{K} \omega_k \eta(X_t|\theta_k) \quad \text{(A2)}$$

where ω_k is the weight parameter of the kth Gaussian, representing the proportion of time that those intensities stay in the image. There is a mixture model for every pixel in the image. Every new pixel value is compared against the existing K Gaussian distributions until a match is found. If none of the distributions match the pixel value, the least probable distribution is replaced with a distribution with the current value as its mean, an initially high variance and low prior weight.

Once all training images are evaluated, the K distributions were ordered based on the criterion ω_k/σ_k, which is proportional to the peak amplitude of the weighted

distribution $\omega_k \eta(X|\theta_k)$. The first B distributions are considered to contain pixel intensity values from the background, where B is estimated as

$$B = \arg\min_b \left(\sum_{k=1}^{b} \omega_k > T \right) \quad \text{(A3)}$$

and T sets the minimum amount of the image that should be identified as background (Table 2). A foreground pixel is any pixel with an intensity more than 2.5 standard deviations away from any of the B distributions.

In analysis of the pixel values in the remaining images of the sequence, the established mixture of K Gaussians continues to be updated using a pre-defined learning rate (Table 2). If a new pixel matches an existing Gaussian in the model its weight, mean and covariance are updated. As in training, if no match is found, a new Gaussian distribution is added. At the end of this process, it is possible to identify, for each pixel, the frames in which the intensity values lie within the first B distributions (background pixels) and the frames in which values lie outside these distributions (foreground pixels).

As fasciculations are typically observed as spatially localized within the muscle (Grimm et al. 2015; Misawa et al. 2011; Pillen et al. 2008; Walker et al. 1990), we expect that frames in which twitch events occur will contain a number of foreground pixels, localized within the image rather than sparsely distributed across the image. To identify clusters of foreground pixels, termed *foreground objects*, the density distribution of the foreground pixels was analysed using connective components. Areas of foreground pixels greater than a minimum value (Table 2) are classed as foreground objects, with all other, more sparsely distributed, foreground pixels disregarded (Stauffer and Grimson 1999). The final result was therefore a 1-D signal of the number of foreground objects at each time point (image frame).

REFERENCES

Arts IM, Overeem S, Pillen S, Kleine BU, Boekestein WA, Zwarts MJ, Jurgen Schelhaas H. Muscle ultrasonography: A diagnostic tool for amyotrophic lateral sclerosis. Clin Neurophysiol 2012;123:1662–1667.

Baumer D, Talbot K, Turner MR. Advances in motor neurone disease. J R Soc Med 2014;107:14–21.

Botter A, Vieira TMM, Loram ID, Merletti R, Hodson-Tole EF. A novel system of electrodes transparent to ultrasound for simultaneous detection of myoelectric activity and B-mode ultrasound images of skeletal muscles. J Appl Physiol 2013;115:1203–1214.

Darby J, Hodson-Tole EF, Costen N, Loram ID. Automated regional analysis of B-mode ultrasound images of skeletal muscle movement. J Appl Physiol 2012;112:313–327.

Darby J, Li B, Costen N, Loram I, Hodson-Tole E. Estimating skeletal muscle fascicle curvature from B-mode Ultrasound image sequences. IEEE Trans Biomed Eng 2013;60:1935–1945.

de Carvalho M, Dengler R, Eisen A, England JD, Kaji R, Kimura J, Mills K, Mitsumoto H, Nodera H, Shefner J, Swash M. Electrodiagnostic criteria for diagnosis of ALS. Clin Neurophysiol 2008;119:497–503.

de Carvalho M, Swash M. Fasciculation discharge frequency in amyotrophic lateral sclerosis and related disorders. Clin Neurophysiol 2016;127:2257–2262.

Fermont J, Arts IMP, Overeem S, Kleine BU, Schelhaas HJ, Zwarts MJ. Prevalence and distribution of fasciculations in healthy adults: Effect of age, caffeine consumption and exercise. Amyotrophic Lateral Scler 2010;11:181–186.

Grimm A, Prell T, Décard BF, Schumacher U, Witte OW, Axer H, Grosskreutz J. Muscle ultrasonography as an additional diagnostic tool for the diagnosis of amyotrophic lateral sclerosis. Clin Neurophysiol 2015;126:820–827.

Hanley JA, McNeil BJ. The meaning and use of the area under a receiver operating characteristic (ROC) curve. Radiology 1982;143:29–36.

Harding PJ, Hodson-Tole EF, Cunningham R, Loram I, Costen N. Automated detection of skeletal muscle twitches from B-mode ultrasound images: An application to motor neuron disease. In: Proceedings, 21st International Conference on Pattern Recognition (ICPR 2012). Piscataway, NJ: IEEE; 2012:2630–2633.

Harding PJ, Loram ID, Combes N, Hodson-Tole EF. Ultrasound-based detection of fasciculations in healthy and diseased muscles. IEEE Trans Biomed Eng 2016;63:512–518.

Jahanmiri-Nezhad F, Barkhaus PE, Rymer WZ, Zhou P. Sensitivity of fasciculation potential detection is dramatically reduced by spatial filtering of surface electromyography. Clin Neurophysiol 2014;125:1498–1500.

Johansson MT, Ellegaard HR, Tankisi H, Fuglsang-Frederiksen A, Qerama E. Fasciculations in nerve and muscle disorders: A prospective study of muscle ultrasound compared to electromyography. Clin Neurophysiol 2017;128:2250–2257.

KaewTraKulPong P, Bowden R. An improved adaptive background mixture model for realtime tracking with shadow detection. 2nd European Workshop on Advanced Video Based Surveillance Systems. Kluwer Academic; 2001:1–5.

Kiernan MC, Vucic S, Cheah BC, Turner MR, Eisen A, Hardiman O, Burrell JR, Zoing MC. Amyotrophic lateral sclerosis. Lancet 2011;377:942–955.

Krämer HH, Vlazak A, Döring K, Tanislav C, Allendörfer J, Kaps M. Excellent interrater agreement for the differentiation of fasciculations and artefacts: A dynamic myosonography study. Clin Neurophysiol 2014;125 2441−2145.

Lucas BD, Kanade T. An iterative image registration technique with an application to stereo vision. In: Proceedings of the 1981 DARPA Image Understanding Workshop. Washington, DC; 1981:121–130.

Maurits NM, Bollen AE, Windhausen A, De Jager AEJ, Van Der Hoeven JH. Muscle ultrasound analysis: Normal values and differentiation between myopathies and neuropathies. Ultrasound Med Biol 2003;29:215–225.

McGill KC, Cummins KL, Dorfman LJ. Automatic Decomposition of the Clinical Electromyogram. IEEE Trans. Biomedical Engineering 1985;32:470–477.

Miguez D, Hodson-Tole EF, Loram I, Harding PJ. A technical note on variable inter-frame interval as a cause of non-physiological experimental artefacts in ultrasound. R Soc Open Sci 2017;4 170245.

Mills KR. Characteristics of fasciculations in amyotrophic lateral sclerosis and the benign fasciculation syndrome. Brain 2010;133:3458–3469.

Misawa S, Noto Y, Shibuya K, Isose S, Sekiguchi Y, Nasu S, Kuwabara S. Ultrasonographic detection of fasciculations markedly increases diagnostic sensitivity of ALS. Neurology 2011;77:1532–1537.

Namburete AIL, Rana M, Wakeling JM. Computational methods for quantifying in vivo muscle fascicle curvature from ultrasound images. J Biomech 2011;44:2538–2543.

Noto Y, Shibuya K, Shahrizaila N, Huynh W, Matamala JM, Dharmadasa T, Kiernan MC. Detection of fasciculations in amyotrophic lateral sclerosis: The optimal ultrasound scan time. Muscle Nerve 2017;56:1068–1071.

Pillen S, Arts IMP, Zwarts MJ. Muscle ultrasound in neuromuscular disorders. Muscle Nerve 2008;37:679–693.

Rana M, Wakeling JM. In-vivo determination of 3D muscle architecture of human muscle using free hand ultrasound. J Biomech 2011;44:2129–2135.

Rana M, Hamarneh G, Wakeling JM. Automated tracking of muscle fascicle orientation in B-mode ultrasound images. J Biomech 2009;42:2068–2073.

Reimers CD, Ziemann U, Scheel A, Rieckmann P, Kunkel M, Kurth C. Fasciculations: Clinical, electromyographic, and ultrasonographic assessment. J Neurol 1996;243:579–584.

Shi J, Tomasi C. Good features to track. In: Proceedings, IEEE Conference on Computer Vision and Pattern Recognition. Piscataway, NJ: IEEE; 1994:593–600.

Stauffer C, Grimson WEL. Adaptive background mixture models for real-time tracking. In: Proceedings, 1999 IEEE Computer Society Conference on Computer Vision and Pattern Recognition (Cat. No PR00149). Piscataway, NJ :IEEE; 1999 ;2:1–252.

Takamatsu N, Nodera H, Mori A, Maruyama-Saladini K, Osaki Y, Shimatani Y, Oda M, Izumi Y, Kaji R. Which muscle shows fasciculations by ultrasound in patients with ALS? J Med Invest 2016;63:49–53.

Tsugawa J, Dharmadasa T, Ma Y, Huynh W, Vucic S, Kiernan MC. Fasciculation intensity and disease progression in amyotrophic lateral sclerosis. Clin Neurophysiol 2018;129:2149–2154.

Tsuji Y, Noto YI, Shiga K, Teramukai S, Nakagawa M, Mizuno T. A muscle ultrasound score in the diagnosis of amyotrophic lateral sclerosis. Clin Neurophysiol 2017;128:1069–1074.

Wagner RF, Smith SW, Sandrik JM, Lopez H. Statistics of speckle in ultrasound B-scans. IEEE Trans Sonics Ultrason 1983;30:156–163.

Walker FO, Donofrio PD, Harpold GJ, Ferrell WG. Sonographic imaging of muscle contraction and fasciculations: A correlation with electromyography. Muscle Nerve 1990;13:33–39.